The reactions of silane in the afterglow of a helium–nitrogen plasma

G R Nowling[1], **S E Babayan**[2], **X Yang**[1], **M Moravej**[1], **R Agarwal**[1] **and R F Hicks**[1]

[1] Chemical Engineering Department, University of California, Los Angeles, CA 90095, USA
[2] Surfx Technologies LLC, 10624 Rochester Ave., Los Angeles, CA 90024, USA

E-mail: rhicks@ucla.edu

Abstract

Optical emission and infrared spectroscopy have been used to study the reactions of nitrogen atoms with silane introduced into the afterglow of an atmospheric-pressure helium–nitrogen plasma. Our experimental observations show that the direct reaction between silane and ground-state nitrogen atoms is slow, with an estimated rate constant no greater than $4 \times 10^{-16}\,\text{cm}^3\,\text{s}^{-1}$, which is 2×10^2–3×10^5 times lower than the values previously reported. Using numerical modelling based on the spectroscopic measurements, we propose that silane dissociation occurs via a two-step process in which energy is first transferred to the molecule from vibrationally excited N_2 and then the activated species collides with N atoms to form SiH_3 and NH. A kinetic model has been developed that allows one to predict the distribution of gas-phase intermediates generated in a remote plasma-enhanced chemical vapour deposition process for silicon nitride.

1. Introduction

Silicon nitride films have a variety of front-end applications in ULSIC manufacturing, including spacers, interlayer dielectrics, diffusion barriers, and novel gate-dielectric stacks [1–4]. For these applications, it is critical that the thermal budget be minimized and that there be no UV or ion-bombardment damage of the transistors. A process showing promise for achieving these goals is remote plasma-enhanced chemical vapour deposition (R-PECVD). Here, the substrate is placed downstream of the discharge, so that it is not directly exposed to the ions and plasma emission. By introducing the silicon precursor into the plasma effluent, the process becomes dominated by the neutral chemistry occurring in the afterglow as well as on the substrate surface.

The R-PECVD of silicon nitride in a helium–nitrogen atmospheric-pressure plasma has been examined in the previous study [5]. Film characteristics different from those achieved in low pressure nitrogen–silane systems were observed. These included a faster deposition rate, good conformality, and hydrogen bonding arrangements favouring nitrogen over silicon. It is generally accepted that the low-pressure process is primarily a surface-dominated process, with little gas-phase chemistry [6–8]. The differences observed in the previous study are attributed to the increased importance of gas-phase reactions at 1 atm, which produce NH_x or $Si_x N_y H_z$ radicals. These species make the atmospheric-pressure N_2–SiH_4 system more like an ammonia–silane R-PECVD process.

The dominant intermediate produced by the helium–nitrogen plasma is ground-state nitrogen atoms, $N(^4S)$ [9, 10]. The concentration of this species in the afterglow is several orders of magnitude higher than that of the electronically excited N_2 molecules (A, B and C states). It would seem logical to conclude that the high-pressure deposition process would be initiated by a reaction between N atoms and silane. However, a review of the literature reveals a large discrepancy in the rate of the reaction between these species. Aubreton *et al* [11] believed that the rate constant for this reaction was extremely high, $1.45 \times 10^{-10}\,\text{cm}^3\,\text{s}^{-1}$. A pure nitrogen dc plasma at 0.2–0.4 Torr was used as the N atom source in this study along with mass spectroscopy to monitor the reaction kinetics. These authors assumed that vibrationally excited molecular nitrogen, $N_2(X, v)$, was quenched by an N_2 buffer gas fed into the afterglow. On the other hand, Piper and Caledonia [12] obtained dramatically different results. They did not observe any evidence of reaction between $N(^4S)$ and silane and gave a maximum rate constant over three orders

of magnitude lower than quoted by Aubreton. They stated, however, that an alternative reaction appeared possible in which energy was transferred from N$_2(X, v)$ to silane prior to N-atom attack.

In this paper, we report our findings on the reactions of silane in the afterglow of an atmospheric-pressure helium–nitrogen plasma. Optical emission spectroscopy (OES) and infrared (IR) absorption spectroscopy have been used to characterize the plasma and monitor the extent of silane conversion in the afterglow. Our results support the findings of Piper in that there appears to be no reaction between N(^{4}S) and silane without first energy transfer from vibrationally excited N$_2$.

2. Experimental methods

The plasma source used in these experiments has been described previously [13]. A schematic of the source is shown in figure 1. It consisted of two parallel electrodes made of aluminium and separated by a gap 1.6 mm across. The upper electrode was 2.2×10.2 cm^2 and was connected to a radio frequency (RF) power supply (13.56 MHz). An aluminium plate, 10.2×10.2 cm^2, was placed downstream of the upper electrode. The lower electrode, measuring 10.2 cm in width and 16.4 cm in length, was grounded and cooled with chilled water. The sides of the gap parallel to the flow direction were sealed with sapphire windows so that IR spectra of the gas could be recorded. The operating conditions of the plasma were fixed at 747.0 Torr He, 13.0 Torr N$_2$, 40.7 litre min^{-1} (measured at 20°C and 1 atm), and 180 W (12 W reflected). All gases entering the system were first passed through oxygen-absorbing purifiers (Matheson Gas Products, 6413).

Silane, at 5.0 vol% in helium, was introduced into the afterglow through one of two linear arrays of 50 holes, each 0.79 mm in diameter. The arrays were located 3 and 14 mm from the plasma discharge boundary, across the width of the lower grounded electrode. These will hence be referred to as the upstream and downstream inlet arrays. The silane mixture, 0.025 to 0.14 total litre min^{-1}, was combined with 1.1–1.4 litre min^{-1} make-up helium to raise the linear velocity out of the holes to 1.0 m s^{-1}. The additional helium greatly increased the rate of silane mixing in the channel. A 0.84 mm rod was placed within 1 mm downstream of whichever array was in use to further improve the mixing. IR spectroscopy was used to obtain the silane absorption spectra along the channel. This was done initially without the plasma ignited
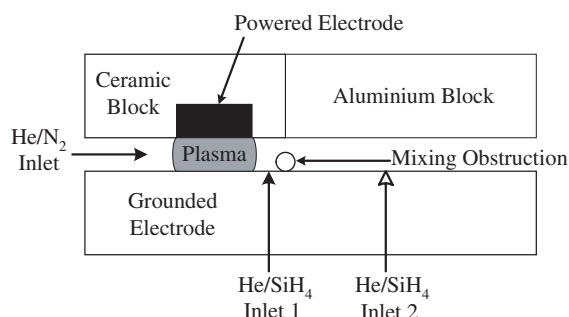
to examine the mixing of silane. These results showed that the silane spectra features were constant at distances $\geqslant 4.5$ mm downstream of the inlet array.
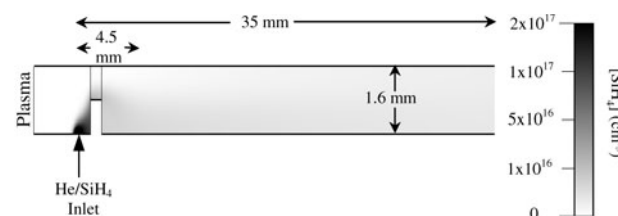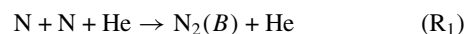
A numerical model of the afterglow was developed using the CFD-ACE software package [14]. The model included all relevant mass and momentum transport phenomena. Shown in figure 2 is a profile obtained for the pure mixing of an ultimate concentration of 4.2×10^{15} cm^{-3} SiH$_4$ injected through the upstream inlet array into the N$_2$–He flow. The silane enters the channel 3 mm downstream of the plasma at a concentration of 1.2×10^{17} cm^{-3} and is diluted by a factor of 30 as it mixes with the plasma effluent. The model validates the IR spectroscopy by predicting a constant silane concentration of 4.2×10^{15} cm^{-3}, averaged over 64 points across the height of the channel, beginning at 4.5 mm downstream of the inlet. The standard deviation at this position is $\pm 2.2 \times 10^{15}$ cm^{-3}, due to the mixing resistance at atmospheric pressure. The mixing improves along the channel nevertheless, with the standard deviation dropping to $\pm 1.0 \times 10^{15}$ and $\pm 0.3 \times 10^{15}$ cm^{-3} at 15 and 35 mm downstream of the inlet.

The methods used to characterize the nitrogen species in the plasma and the afterglow have been described in more detail elsewhere [9, 10]. Briefly, a monochromator (Instruments S.A., Triax 320) equipped with a charge-coupled device (Instruments S.A., CCD-3000) and photo-multiplier tube (Hamamatsu, R928P) was positioned at the outlet of the discharge. In the plasma, the concentrations of N$_2(B)$, vibrational levels 0 to 12, and N$_2(C)$, vibrational levels 0 to 4, were determined from the intensities of the emission bands measured with the CCD and using known Einstein coefficients [10]. The CCD detector was calibrated with a standard tungsten lamp (Oriel, 63976). The transient decay of the N$_2(B)$ and N$_2(C)$ emission after turning the plasma off was measured with the PMT and an oscilloscope (Tektronix TDS 224). For these latter experiments, the RF power was delivered in 100 ms pulses with a 20% duty cycle. A power sampler monitored the voltage signal and triggered the oscilloscope. The initial state for these temporal decay profiles was set equal to the concentrations measured in the plasma with the CCD. Concentration profiles for N$_2(A, v = 0$ and 1) were obtained from a material balance on the N$_2(C, v)$ species [10].

The atomic nitrogen concentration was calculated from the transient intensities of the N$_2(B, v)$ signals using the following relation derived in the previous paper [9]:

$$[N(t)] = \frac{-\mathrm{d} \ln I_{N_2(B,v)}(t)/\mathrm{d}t}{4k_{recomb}(He)[He]} \quad (1)$$

where k_{recomb} is the rate constant for the three-body recombination reaction

$$N + N + He \rightarrow N_2(B) + He \quad (R_1)$$

Figure 1. Schematic of the atmospheric-pressure plasma source, set to deliver silane through the upstream silane inlet array.

**Figure 2.** Simulation of silane mixing in the afterglow using the CFD-ACD program [14].

This is the primary consumption mode of nitrogen atoms in the afterglow. The value of k_{recomb} is $2.2^{+2.2}_{-0.7} \times 10^{-33}$ cm^6 s^{-1} [9]. This method of obtaining the N-atom density from OES of the N$_2$(B) state is well established [15–17]. Furthermore, in our earlier work we verified the N-atom predictions from equation (1) by comparison with nitric oxide titration [9]. This equation could not be used to characterize the N-atom density in the presence of silane as SiH$_4$ is a highly efficient quencher of N$_2$(B) [18]. Consequently, the rate of the reaction between N(^{4}S) and SiH$_4$ was examined using silane measurements.

A Fourier-transform IR spectrometer (BioRad FTS-7) was used to monitor silane consumption in the afterglow. This technique has been used to measure silane and methane dissociation in plasma systems [19–21]. The IR beam from the spectrometer was passed between the two plates at various points along the afterglow. The spectra were collected with a mercury–cadmium–telluride detector at a resolution of 1 cm^{-1} and signal averaging of 16 scans. A 0.75 mm slit was placed between the plasma source and detector, resulting in a position resolution estimated to be ± 1.5 mm. The procedure for taking the IR spectra was to take a single-beam scan of the He–N$_2$ mixture. Next, silane was added and another single-beam scan taken. These two spectra were used to construct a 'plasma off' silane absorbance spectrum. Next the plasma was ignited and a third spectrum taken, followed by a fourth with the plasma and silane turned off. These two single-beam spectra were combined to create a 'plasma on' absorbance spectrum. The purpose of the final scan was to eliminate any possible contributions from deposition on the windows. An ungrounded thermocouple was inserted into the afterglow to measure the temperature increase with the plasma at each scanning position.

3. Results and discussion

3.1. Nitrogen plasma characterization

Shown in figure 3 are the decay profiles for the nitrogen species with no mixing obstruction in place. The purpose of leaving out the obstruction was to illustrate how the intermediates decay as the gas travels from the plasma to the upstream and downstream silane inlet arrays. The temporal results obtained from the PMT are mapped onto the position scale
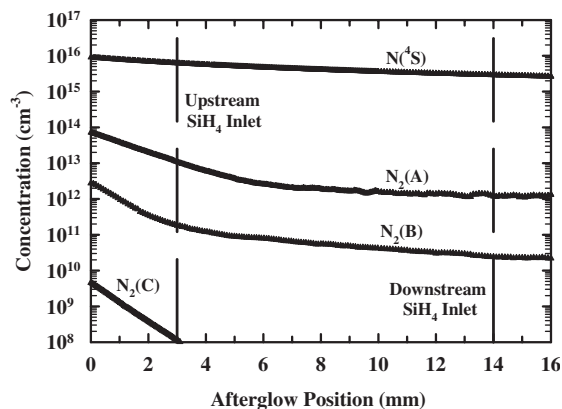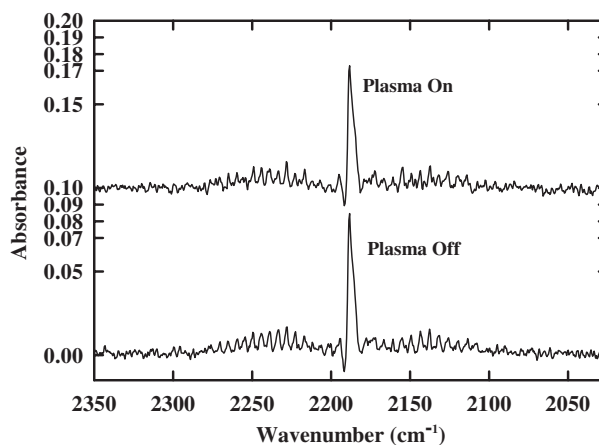
by multiplying the time by an average linear velocity of the gas in the channel, which is constant without the obstruction in place. The concentrations at the plasma exit are as follows: 9.0×10^{15} cm^{-3} N(^{4}S), 7.5×10^{13} cm^{-3} N$_2$(A), 2.1×10^{12} cm^{-3} N$_2$(B), and 8.0×10^{10} cm^{-3} N$_2$(C). The estimated accuracy of these measurements is $\pm 20\%$ for each species [10]. Clearly, atomic nitrogen is the dominant reactive intermediate in the plasma and afterglow. Its density is 10^2–10^5 times that of the other species. Also, the N atoms decay slowly, falling only to 3×10^{15} cm^{-3} at the downstream silane inlet array. This is due to the fact that the three-body recombination rate of the N atoms is much less than the quenching rate of N$_2$(A), N$_2$(B), and N$_2$(C) [9, 10].

It is important that the N atoms not be consumed by collisions with the mixing obstruction. This should not occur to a significant extent since the wall recombination coefficient is low, 8×10^{-4}–3×10^{-6} per wall collision [22]. The N-atom longevity was confirmed by examining the N$_2$(B) concentration downstream of the obstruction. The N$_2$(B) decay profiles taken with the obstruction in place had the same shape and features as those shown in figure 3. If the N atoms were being consumed by wall collisions, the N$_2$(B) concentration profile downstream of the obstruction would have been noticeably steeper, not stabilizing at $\sim 1 \times 10^{10}$ cm^{-3}.
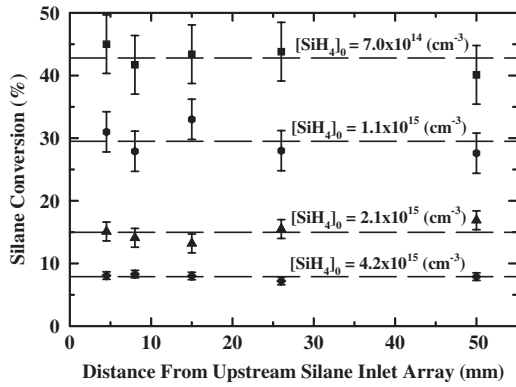
3.2. Silane conversion measurements

IR absorption spectra of gas-phase silane are shown in figure 4. The peak at ~ 2190 cm^{-1} is due to the Q-branch of the SiH$_4$ v_3 mode [21, 23]. With the plasma off, the silane density in the duct 4.5 mm downstream of the inlet array is 4.2×10^{15} cm^{-3}. This yields a v_3 peak height of approximately 0.085 abs. units. The height of this peak scales linearly with concentration over the range of silane flows used. When the plasma is turned on, the v_3 peak height decreases by 10.7%. After accounting for the small (<10 K) temperature increase with the plasma on versus off, this drop corresponds to a silane conversion of 8.2%.

For the silane conversion measurement to be valid, the IR spectrum must not be affected by reaction products generated in the afterglow. One species that could affect the vibrational data is Si$_2$H$_6$. Disilane is long lived and produces a broad absorbance peak at ~ 2150 cm^{-1} [21, 24, 25]. Nevertheless, as shall be shown later, the disilane formed in the afterglow is

Figure 3. Concentration profiles for N(^{4}S), N$_2$(A), N$_2$(B), and N$_2$(C) with no mixing obstruction in place. The zero position on the x-axis corresponds to the plasma/afterglow boundary.

Figure 4. IR absorption spectra with and without the plasma on.

Figure 5. Silane conversion profiles along the afterglow for inlet concentrations between 7.0×10^{14} and 4.2×10^{15} cm^{-3}.
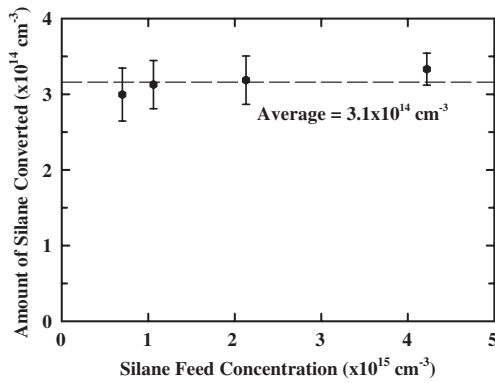

Figure 6. The amount of silane consumed by reaction with the He–N₂ plasma afterglow as a function of the feed concentration.

over a factor of 4 below the detection limit of the apparatus. Reactive SiH$_x$ radicals are difficult to detect by IR absorption, typically requiring high-resolution (>0.005 cm^{-1}) laser diode spectroscopy [21, 26–28]. Consequently, we expect little contribution from these radicals in the silane vibrational spectrum.

Silane conversion profiles along the channel are shown in figure 5. The conditions are 7×10^{14}–4.2×10^{15} cm^{-3} SiH₄ introduced through the upstream inlet array. The first feature of note is that there is no measurable rise in conversion with position from 4.5 to 50.0 mm. Rather, the conversion achieves a constant value within 4.5 mm downstream of the silane inlet array in each case. A second notable feature of the data in figure 5 is that the conversion values follow the SiH₄ concentration trend inversely, i.e. when the concentration is doubled, the conversion is halved. This trend is better illustrated in figure 6, in which the amount of silane consumed for each inlet condition is shown. From this figure, it is clear that $\sim 3.1 \times 10^{14}$ cm^{-3} of silane is converted for every inlet condition examined. Finally, no reduction in the v_3 mode is observed either when no nitrogen is fed to the plasma or when the silane is introduced through the downstream silane inlet array.

3.3. Numerical modelling

A number of observations can be made from the experimental data presented thus far. From figures 5 and 6 we can see that the
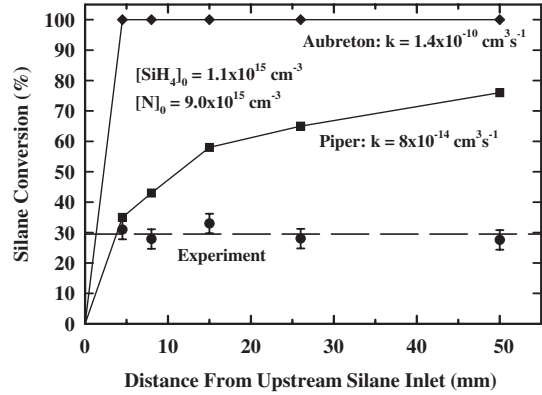

Figure 7. Experimental and calculated silane conversion profiles with an inlet SiH₄ concentration of 1.1×10^{15} cm^{-3}.

silane is undergoing a reaction that consumes $\sim 3.1 \times 10^{14}$ cm^{-3} of SiH₄ and reaches completion within 4.5 mm of the upstream silane array. The species that silane is reacting with must be some form of nitrogen, as shown by the fact that no conversion is observed without any N₂ fed to the discharge. This eliminates the possibility of a helium species or unknown impurity being responsible for the silane reaction.

It appears unlikely that the silane is directly reacting with N atoms. As shown in figure 3, the decay rate of the nitrogen atoms is slow, only falling by a factor of 2 from the upstream to downstream silane inlet arrays. The concentration of the N(^{4}S) at the downstream set of holes is 3×10^{15} cm^{-3}, which is still higher than three of the four silane densities used in this study. Thus, almost no change in the silane conversion should occur upon switching its entry point from the upstream to the downstream inlet array. However, this is not observed experimentally as the conversion drops to below the detection limit upon feeding the SiH₄ 14 mm beyond the N₂ discharge boundary.

Shown in figure 7 is the experimental silane conversion profile along with two profiles predicted by the CFD-ACE model with the reactions

$$N + N + He \rightarrow N_2(B) + He \qquad (R_1)$$

and

$$N + SiH_4 \rightarrow products \qquad (R_2)$$
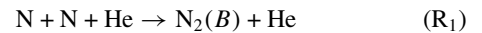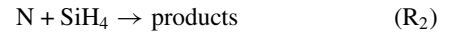
The two numerical profiles are obtained using the (R_2) rate constants obtained by Aubreton et al and Piper and Caledonia [11, 12]. The CFD model has been used in order to account for the mixing occurring in the flow system. The cases shown in figure 7 are with 1.1×10^{15} cm^{-3} of silane introduced through the upstream array of holes. The rate constant predicted by Aubreton is sufficiently high that all the silane is consumed within 4.5 mm from the entry point. The maximum rate coefficient obtained by Piper is over three orders of magnitude smaller and thus predicts a slow, measurable rise in conversion. However, the rate constant is large enough that $\sim 75\%$ of the silane should be consumed within 50.0 mm from the entry point. Our experimental results cannot be explained using either Aubreton or Piper's kinetics. Evidently, the silane undergoes a fast reaction with an active nitrogen species that is present at a concentration of about 3×10^{14} cm^{-3} at the

upstream silane inlet array. This comparison, along with the strong effect of the silane inlet position, confirms that the SiH$_4$ does not react directly with N atoms.

From figure 7, the rate constant for any direct N + SiH$_4$ reaction must be less than 8×10^{-14} cm^3 s^{-1}. Otherwise, the SiH$_4$ conversion measured at 4.5 mm would not equal that at 50.0 mm. We can obtain a new upper bound for this rate constant by considering the experiments with the largest silane concentration, 4.2×10^{15} cm^{-3}, since it generates the fastest forward rate. The error in each silane conversion measurement at this condition is $\pm 0.5\%$. Using the model, the rate constant for any direct N + SiH$_4$ reaction must be less than 4×10^{-16} cm^3 s^{-1} for the per cent conversion at 50.0 mm to be within 1% (twice the error) of that at 4.5 mm. This reduces the previously known upper bound for this reaction by a factor of 200 [12].

The nitrogen intermediate that is reacting with the silane still remains to be identified. The electronically excited nitrogen molecules may be eliminated because their concentrations are too low, $<9 \times 10^{12}$ cm^{-3}, to account for the silane conversions observed. A likely candidate for the unknown species is vibrationally excited molecular nitrogen, $N_2(X, v)$ [12]. It is possible to estimate the $N_2(X, v \geqslant 4)$ density in the afterglow using a mass balance on $N_2(B, v = 0$ to 12) and the profiles shown in figure 3. A similar method was used by Diamy *et al* [29] to estimate vibrationally excited nitrogen densities. The reactions used in the $N_2(B)$ material balance are shown in table 1. In the early afterglow, the $N_2(B)$ consumption pathways (R$_4$) and (R$_5$) are balanced by production from three-body N-atom recombination (R$_1$) and $N_2(A)$ energy pooling with either another $N_2(A)$ molecule (R$_3$) or $N_2(X, v \geqslant 4)$ (R$_7$). We have only used this method to estimate the $N_2(X, v \geqslant 4)$ density within the first millisecond (4 mm) of the afterglow. Shown in figure 8 is the predicted $N_2(X, v \geqslant 4)$ concentration profile starting at the end of the plasma discharge and into the afterglow. The data points (∇) extending to 4 mm are the results of the $N_2(B)$ material balance. The dotted vertical lines show the location of the silane inlet arrays.

Beyond 4 mm into the afterglow, the $N_2(A)$ concentration drops by two orders of magnitude, and the production pathways (R$_3$) and (R$_7$) become insignificant next to (R$_1$) [9]. However, by assuming that the dominant mode of $N_2(X, v \geqslant 4)$ loss is helium quenching, we can fit the decay profile and extend it further into the afterglow. The fit, shown by the solid

line in figure 8, yields a He quenching rate constant of 1.8×10^{-16} cm^3 s^{-1}. This value is in good agreement with unpublished results obtained at Physical Sciences, Inc. [34]. These studies also indicated that wall quenching of $N_2(X, v)$ is inefficient, with a quenching probability of 1×10^{-4} per wall collision. Using this value, we estimate the loss due to wall quenching over the region 4.5 mm downstream of the silane inlet, including the mixing obstruction, to be approximately a hundredth of the number of molecules contained in that volume. Thus, the $N_2(X, v)$ density should not be appreciably reduced by collisions with the channel walls and mixing obstruction.

Using only helium quenching to extend the $N_2(X, v \geqslant 4)$ profile yields a lower bound of the late afterglow concentrations since there would be some $N_2(X, v)$ production from the decay of electronically excited species. As an upper bound for the density, a simulation was run that assumed that all quenched $N_2(A)$ went into the $N_2(X, v \geqslant 4)$ state. This fit is shown as the dashed line in figure 8. The actual $N_2(X, v \geqslant 4)$ concentration profile in the late afterglow should lie somewhere between these two fits.

From figure 8, the estimated $N_2(X, v \geqslant 4)$ density at the plasma-afterglow boundary is 1×10^{16} cm^{-3}. At the upstream silane inlet array, the concentration drops to 8×10^{14} cm^{-3}. By the time the effluent has reached the downstream array, the $N_2(X, v \geqslant 4)$ density drops to between 2×10^{13} and 1×10^{11} cm^{-3} as predicted by the two decay models discussed above. This occurs despite the relatively small helium-quenching rate constant because of the high helium pressure in the system. The drop by more than an order of magnitude in $N_2(X, v \geqslant 4)$ concentration mirrors the lack of silane conversion observed at the downstream inlet array. With this method, it is not possible to obtain a more specific distribution of the nitrogen vibrational levels. However, based on the density profile of $N_2(X, v \geqslant 4)$, vibrationally excited nitrogen is most likely the species that reacts with silane in the afterglow.

It has been shown by Piper [18] that the rate of $N_2(X, v)$ quenching by silane is efficient, with a rate coefficient lower bound of 6×10^{-13} cm^3 s^{-1}. In his previous study, there was no indication that the silane was dissociated by the energy transfer reaction [34]. Rather, the excited silane simply relaxed or was quenched back down to the ground state. A notable aspect of his study is that the nitrogen atoms were eliminated from

Table 1. Production and consumption reactions used in the $N_2(B)$ mass balance to obtain the $N_2(X, v \geqslant 4)$ density profile.
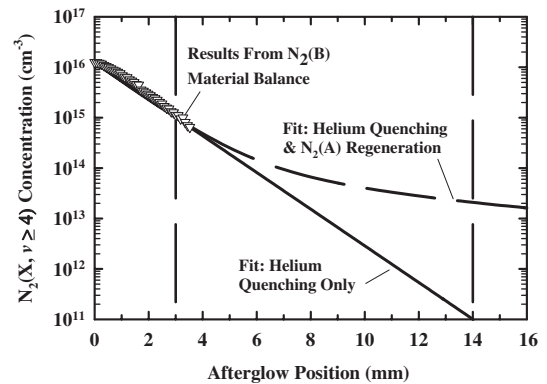
	Reaction	Rate constant at 303 K (cm^3 s^{-1})	Ref.
(R$_1$)	N + N + He $\rightarrow N_2(B)$ + He	2.2×10^{-33} cm^6 s^{-1}	[9, 10]
(R$_3$)	$N_2(A) + N_2(A)$ $\rightarrow N_2(B) + N_2$	1.1×10^{-9}	[30]
(R$_4$)	$N_2(B) \rightarrow N_2(A) + h\nu$	1.5×10^{5} s^{-1}	[31]
(R$_5$)	$N_2(B)$ + He $\rightarrow N_2(\neq B)$ + He	1.2×10^{-12}	[32]
(R$_6$)	$N_2(C) \rightarrow N_2(B) + h\nu$	3.0×10^{7} s^{-1}	[31]
(R$_7$)	$N_2(A) + N_2(X, v \geqslant 4)$ $\rightarrow N_2(B) + N_2$	4×10^{-11}	[33]

Figure 8. The dependence of the concentration of the vibrationally excited N$_2$ molecules on position in the afterglow. The dotted lines indicate the silane inlet points.

the afterglow before silane introduction. In this work, any energy exchange between N$_2(X, v)$ and silane occurs in the presence of a high N-atom density. Dissociation of the silane may occur then by a two-step process, the first step being energy transfer between N$_2(X, v)$ and silane and the second step being dissociation of the excited silane by N(^{4}S):

$$N_2(X, v) + SiH_4 \rightarrow N_2(X, v' < v) + SiH_4^* \qquad (R_8)$$

$$N(^4S) + SiH_4^* \rightarrow NH + SiH_3. \qquad (R_9)$$
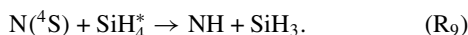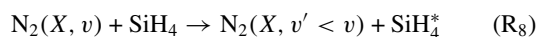
If in reaction (R$_9$) the silane were in its ground state, this step would be endothermic by 0.45 eV [12]. However, the transfer of two quanta of N$_2$ vibrational energy to the silane is sufficient to make the reaction exothermic [12, 35]. Obviously, the rate of (R$_9$) must be fast enough so that the excited silane does not get quenched by helium. We can use this condition to make a rough estimate of the rate constant for (R$_9$). The rate coefficient for excited silane quenching by argon has been found to be 6×10^{-15} cm^3 s^{-1} [18]. Assuming this value holds for helium, the minimum rate constant of (R$_9$) would then have to be of the order of 1×10^{-11} cm^3 s^{-1} to exceed the rate of helium quenching. An upper bound of 6×10^{-10} cm^3 s^{-1} for (R$_9$) can be obtained for N and SiH$_4$ from hard-sphere collision theory [36].

As demonstrated in Piper's N$_2(X, v)$-SiH$_4$ kinetic study, ~15% of the silane involved in reaction (R$_8$) can undergo v_3 excitation [18]. This corresponds to a SiH$_4^*(v_3)$ density of ~4.7×10^{13} cm^{-3}. In spite of its small concentration, it is theoretically possible that emissions from v_3-excited silane could interfere with the IR conversion measurements. However, were any SiH$_4^*(v_3)$ emissions still present and interfering with the IR spectra taken 4.5 mm downstream of the silane inlet, the silane conversions measured at this position would not equal those obtained further down the channel. The fact that there is agreement at all positions sampled indicates that any excited silane must be consumed within 4.5 mm of the silane inlet. The excited silane can therefore be thought of as a short-lived, reactive intermediate.

The importance of vibrationally excited nitrogen in the reaction between N(^{4}S) and SiH$_4$ could account for the discrepancy in the rate coefficients found in the literature. As mentioned earlier, the study by Aubreton relied on N$_2$ quenching to eliminate N$_2(X, v)$ from the afterglow [11]. However, it has been shown that N$_2$ is an inefficient quencher of N$_2(X, v)$ [37–39]. Thus it is possible that vibrationally excited nitrogen was present in the system of the authors, causing them to observe an erroneously high rate coefficient for the direct reaction between N(^{4}S) and silane.

With a better understanding of the initiation steps, kinetic modelling can be used to identify the products generated in the afterglow. Presented in table 2 is a proposed mechanism based on our results, combined with a group of elementary reactions obtained from the literature. After the initiation process (R$_8$) and (R$_9$), the product NH radicals undergo a reaction with excess N atoms (R$_{11}$), thereby producing atomic hydrogen. The H atoms can dissociate a portion of the unreacted silane and the SiH$_3$ radicals, among other possible pathways (R$_{12}$) to (R$_{18}$). Recombination of the SiH$_x$ and NH$_x$ radicals leads to the formation of higher-order silanes and amino-silanes (R$_{20}$) to (R$_{24}$).
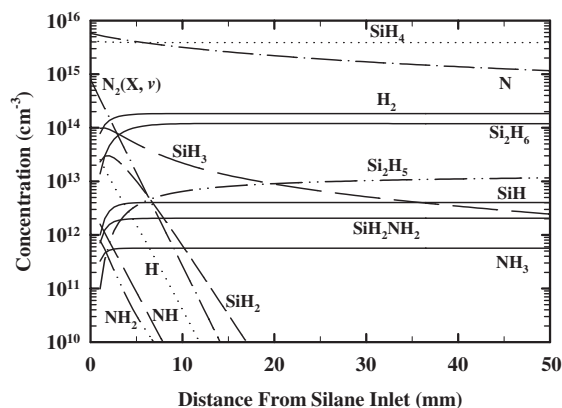
The concentration profiles predicted by the reaction mechanism for an initial silane density of 4.2×10^{15} cm^{-3} are shown in figure 9. The predicted silane conversion agrees with that observed by IR spectroscopy. The dominant stable products are molecular hydrogen and disilane. The latter product, with a concentration of 1.3×10^{14} cm^{-3}, accounts for 87% of the silane converted. Using published disilane spectra and absorption coefficients [21, 24, 25], we calculate a detection limit of 6×10^{14} cm^{-3} in the range of 2000–2400 cm^{-1}. Therefore, it may be concluded that the presence of disilane in the afterglow does not affect the IR absorption measurements for silane. The other silyl reaction products of note are Si$_2$H$_5$, SiH$_3$, SiH, and SiH$_2$NH$_2$, which account for 7.5%, <0.5%, 2.7%, and 2.3% of the SiH$_4$ converted, respectively.

The results shown in figure 9 can also be used to explain key observations in our atmospheric-pressure silicon nitride

Table 2. Proposed gas-phase reaction mechanism for silane conversion during R-PECVD.

	Reaction	Rate constant at 303 K (cm^3 s^{-1})	Ref.
(R$_1$)	N + N + He $\rightarrow$ N$_2$(B) + He	2.2×10^{-33} cm^6 s^{-1}	[9, 10]
(R$_{10}$)	N$_2$(X, v) + He $\rightarrow$ N$_2$($X, v' < v$) + He	~2×10^{-16}	Est. (see text)
(R$_8$)	N$_2$(X, v) + SiH$_4$ $\rightarrow$ N$_2$($X, v' < v$) + SiH$_4^*$	$>6 \times 10^{-13}$	[18]
(R$_9$)	N + SiH$_4^*$ $\rightarrow$ NH + SiH$_3$	1×10^{-11}–6×10^{-10}	Est. (see text)
(R$_{11}$)	NH + N $\rightarrow$ N$_2$ + H	5.0×10^{-11}	[40, 41]
(R$_{12}$)	NH + H $\rightarrow$ H$_2$ + N	3.5×10^{-11}	[40, 41]
(R$_{13}$)	NH + H + He $\rightarrow$ NH$_2$ + He	9.5×10^{-30} cm^6 s^{-1}	[40, 41]
(R$_{14}$)	H + H + He $\rightarrow$ H$_2$ + He	9.1×10^{-33} cm^6 s^{-1}	[42]
(R$_{15}$)	H + SiH$_4$ $\rightarrow$ SiH$_3$ + H$_2$	2.7×10^{-12}	[43]
(R$_{16}$)	H + SiH$_3$ $\rightarrow$ SiH$_2$ + H$_2$	3.9×10^{-13}	[43]
(R$_{17}$)	H + SiH$_2$ $\rightarrow$ SiH + H$_2$	8.0×10^{-13}	[44]
(R$_{18}$)	NH$_2$ + H + He $\rightarrow$ NH$_3$ + He	6.1×10^{-30} cm^6 s^{-1}	[45]
(R$_{19}$)	SiH$_3$ + SiH$_3$ $\rightarrow$ SiH$_2$ + SiH$_4$	7.0×10^{-12}	[43]
(R$_{20}$)	SiH$_3$ + SiH$_3$ $\rightarrow$ Si$_2$H$_6$	1.0×10^{-11}	[43]
(R$_{21}$)	SiH$_4$ + SiH$_2$ $\rightarrow$ Si$_2$H$_6$	1.0×10^{-11}	[43]
(R$_{22}$)	Si$_2$H$_6$ + SiH$_3$ $\rightarrow$ SiH$_4$ + Si$_2$H$_5$	1.0×10^{-12}	[43]
(R$_{23}$)	Si$_2$H$_6$ + H $\rightarrow$ H$_2$ + Si$_2$H$_5$	2.2×10^{-12}	[43]
(R$_{24}$)	NH$_2$ + SiH$_3$ $\rightarrow$ SiH$_2$NH$_2$ + H	1.0×10^{-10}	[46]

Reactions (R$_{20}$) and (R$_{21}$) are for the overall reaction that includes the quenching of the excited disilane molecule.

Figure 9. Concentration profiles for the species present in the afterglow of an atmospheric-pressure N_2–He–SiH_4 R-PECVD process, as predicted by the reaction mechanism presented in table 2.

R-PECVD study [5]. The strongest effect on the deposition rate was from the distance the gas mixture travels before impinging on the wafer, with the rate falling sharply from 1100 to 0 Å min^{-1} over a distance of 15 mm [5]. The gas velocity in the R-PECVD study is approximately equal to that used in this work. Upon examination of figure 9, we find that the SiH_3 radical exhibits a large drop in concentration over this same distance, i.e. from 1.0×10^{14} to 1.0×10^{13} cm^{-3}. This suggests that SiH_3 plays a pivotal role in the PECVD process, consistent with prior work [48–52]. Another interesting result from our study of silicon nitride R-PECVD at atmospheric-pressure was the dominance of N–H over Si–H bonding in the film. This is unexpected when the nitrogen precursor fed to the plasma is N_2 as opposed to NH_3 [5, 53–55]. We suspect that this may be due to the formation of SiH_2NH_2 radicals, as shown in figure 9.

4. Conclusions

We have observed that the direct reaction between N(^{4}S) and silane is slow, with a maximum rate constant of 4×10^{-16} cm^3 s^{-1}. Numerical modelling based on our experimental results suggests that silane dissociation occurs rather via a two-step process. The first step involves energy transfer from vibrationally excited N_2 to SiH_4, while the second step is the reaction between the activated SiH_4 and ground-state N atoms. Additional work is currently under way to verify this mechanism experimentally.

Acknowledgments

References

[1] Yota J, Handler J and Saleh A A 2000 *J. Vac. Sci. Technol.* A **18** 372
[2] Jaeger R C 1993c Modular series on solid state devices *Introduction to Microelectronic Fabrication* vol 5 (Reading, MA: Addison-Wesley)
[3] Sze S M 1985c *Semiconductor Devices* (New York: Wiley)
[4] Lucovsky G, Wu Y, Niimi H, Yang H, Keister J and Rowe J E 2000 *J. Vac. Sci. Technol.* A **18** 1163
[5] Nowling G R, Babayan S E, Jankovic V and Hicks R F 2002 *Plasma Sources Sci. Technol.* **11** 97
[6] Kushner M J 1992 *J. Appl. Phys.* **71** 4173
[7] Smith D L, Alimoda A S and von Presissig F J 1990 *J. Vac. Sci. Technol.* B **8** 551
[8] Smith D L 1993 *J. Vac. Sci Technol.* A **11** 1843
[9] Babayan S E, Ding G and Hicks R F 2001 *Plasma Chem. Plasma Process.* **21** 505
[10] Babayan S E, Ding G, Nowling G R, Yang X and Hicks R F 2002 *Plasma Chem. Plasma Process.* **22** 255
[11] Aubreton J, Conte D, Jauberteau J L and Jauberteau I 2000 *J. Phys. D: Appl. Phys.* **33** 1499
[12] Piper L G and Caledonia G E 1991 *J. Phys. Chem.* **95** 698
[13] Yang X, Babayan S E and Hicks R F 2003 *Plasma Sources Sci. Technol.* submitted
[14] CFD-ACE software package, see www.cfdrc.com
[15] Noxon J F 1962 *J. Chem. Phys.* **36** 926
[16] Campbell I M and Thrush B A 1967 *Proc. R. Soc.* A **296** 201
[17] Young R A and Black G 1965 *J. Chem. Phys.* **44** 3741
[18] Piper L G 2002 *J. Phys. Chem.* A **106** 8355
[19] Sansonnens L, Howling A A and Hollenstein C 1998 *Plasma Sources Sci. Technol.* **7** 114
[20] van Hest M F A M, de Graaf A, van de Sanden M C M and Schram D C 2000 *Plasma Sources Sci. Technol.* **9** 615
[21] Morrison P W Jr and Haigis J R 1993 *J. Vac. Sci. Technol.* A **11** 490
[22] Wei T, Collins L R and Phillips J 1996 *AIChE J.* **42** 1361
[23] Wilkinson G R and Wilson M K 1996 *J. Chem. Phys.* **44** 3867
[24] Bethke G W and Wilson M K 1957 *J. Chem. Phys.* **26** 1107
[25] Gutowsky H S and Stejskal E O 1954 *J. Chem. Phys.* **22** 939
[26] Yamada C, Kanamori H, Hirota E, Nishiwaki N, Itabashi N, Koto K and Goto T 1989 *J. Chem. Phys.* **91** 4582
[27] Davies P B, Isaacs N A, Johnson S A and Russell D K 1985 *J. Chem. Phys.* **83** 2060
[28] Chollet P, Guelachvili G and Chapey M 1986 *J. Opt. Soc. Am.* B **3** 687
[29] Diamy A M, Hochard L, Legrand J C and Ricard A 1998 *Plasma Chem. Plasma Process.* **18** 447
[30] Nadler I and Rosenwaks S 1985 *J. Chem. Phys.* **83** 3932
[31] Gilmore F R, Laher R R and Espy P 1992 *J. Phys. Chem. Ref. Data* **21** 1005
[32] Ionikh Y Z and Chernysheva N V 1990 *Opt. Spectrosc. (USSR)* **68** 598
[33] Piper L G 1994 *J. Chem. Phys.* **101** 10229
[34] Piper L G private communication
[35] Golde M F and Thrush B A 1972 *Faraday Discuss. Chem. Soc.* **53** 52
[36] Levine I N 1995c *Physical Chemistry* (New York: McGraw-Hill)
[37] Piper L G 1992 *J. Chem. Phys.* **97** 270
[38] Hwang H H and Kushner M J 1994 *Plasma Sources Sci. Technol.* **3** 190
[39] Dhali S K 1989 *Trans. Plasma Sci.* **17** 603
[40] Davidson D F, Kohse-Hoinghaus K, Chang A Y and Hanson R K 1990 *Int. J. Chem. Kinet.* **22** 513
[41] Hanson R K and Salimian S 1984c *Combustion Chemistry* (New York: Springer)
[42] Miller J A and Melius C F 1992 *Combust. Flame* **91** 21
[43] Kushner M J 1988 *J. Appl. Phys.* **63** 2532
[44] Coltrin M E, Kee R J and Miller J A 1986 *J. Electrochem. Soc.* **133** 1206
[45] Gordon S, Mulac W and Nangia P 1971 *J. Phys. Chem.* **75** 2087
[46] Beach D B and Jasinski J M 1990 *J. Phys. Chem.* **94** 3019
[47] Kessels W M M, Hoefnagels J P M, Boogaarts M G H, Schram D C and van de Sanden M C M 2001 *J. Appl. Phys.* **89** 2065
[48] Moravej M, Babayan S E, Nowling G R, Yang X and Hicks R F 2004 *Plasma Sources Sci. Technol.* **13** 8

[49] Robertson J 2000 *J. Appl. Phys.* **87** 2608
[50] Matsuda A 1999 *Thin Solid Films* **337** 1
[51] Robertson R and Gallagher A 1986 *J. Chem. Phys.* **85** 3623
[52] Kessels W M M, Smets A H M, Marra D C, Aydil E S, Schram D C and van de Sanden M C M 2001 *Thin Solid Films* **383** 154
[53] Alexandrov S E, Hitchman M L and Shamlian S 1993 *Adv. Mater. Opt. Electron.* **2** 301
[54] Theil J A, Hattangady S V and Lucovsky G 1992 *J. Vac. Sci. Technol.* A **10** 719
[55] Lucovsky G, Richard P D, Tsu D V, Lin S Y and Markunas R J 1986 *J. Vac. Sci. Technol.* A **4** 682